HHS Public Access

Author manuscript

Acta Biomater. Author manuscript; available in PMC 2019 April 15.

Published in final edited form as:

Acta Biomater. 2018 April 15; 71: 118–131. doi:10.1016/j.actbio.2018.03.003.

Inhibition of osteoclastogenesis by stem cell-derived extracellular matrix through modulating the intracellular reactive oxygen species

Mao Li[a,b,1], **Xi Chen**[a,b,c,1], **Jinku Yan**[a,b,1], **Long Zhou**[a,b], **Yifan Wang**[a,b], **Fan He**[a,b,*], **Jun Lin**[a], **Caihong Zhu**[a,b], **Guoqing Pan**[a,b], **Jia Yu**[a,b], **Ming Pei**[d], **Huilin Yang**[a,b], and **Tao Liu**[a,**]

[a]Department of Orthopaedics, The First Affiliated Hospital of Soochow University, Suzhou 215006, China

[b]Orthopaedic Institute, Medical College, Soochow University, Suzhou 215007, China

[c]School of Biology and Basic Medical Sciences, Medical College, Soochow University, Suzhou 215123, China

[d]Stem Cell and Tissue Engineering Laboratory, Department of Orthopaedics and Division of Exercise Physiology, West Virginia University, Morgantown, WV 26506, USA

Abstract

Decellularized extracellular matrix (ECM) derived from stem cells has been shown as a promising biomaterial for bone regeneration because of the promotion effect on osteogenesis in mesenchymal stem cells (MSCs). However, bone regeneration is also influenced by bone resorption and little is known about the effect of cell-derived ECM on osteoclast differentiation. In this study, ECM was deposited by MSCs and, after decellularization, the effect of ECM on osteoclastogenesis of bone marrow monocytes (BMMs) was investigated in comparison to standard tissue culture polystyrene. Our results showed that cell-derived ECM improved BMM proliferation but potently inhibited osteoclast differentiation, evidenced by down-regulation of multinucleated tartrate-resistant acid phosphatase (TRAP)-positive cells, areas of actin rings, and osteoclast-specific gene expression. ECM-mediated attenuation of intracellular reactive oxygen species (ROS) was suggested to play a rival role in the inhibition of osteoclastogenesis, because

*Fan He, Ph.D., Orthopaedic Institute, Soochow University, No.708 Renmin Road, Suzhou 215007, Jiangsu, China. Telephone: +86-512-67781420; Fax: +86-512-67781165; fanhe@suda.edu.cn. **Tao Liu, M.D., Ph.D., Department of Orthopaedics, The First Affiliated Hospital of Soochow University, No. 188 Shizi Street, Suzhou 215006, Jiangsu, China. Telephone: +86-512-67781420; Fax: +86-512-67781165; liutao8250@163.com.

[1]Mao Li, Xi Chen, and Jinku Yan contributed equally to this work.

Conflicts of Interest

The authors declare that they have no conflicts of interest.

Author Contributions

Mao Li, Xi Chen, Jinku Yan, and Fan He designed the research study; Mao Li, X C, Jinku Yan, Long Zhou, Yifan Wang, Caihong Zhu, Guoqing Pan, Tao Liu, and Fan He performed the experiments; Xi Chen, Jun Lin, Jia Yu, and Fan He analyzed the data; Tao Liu and Fan He wrote the paper; Huilin Yang and Ming Pei participated in the conception of the study and revision of the manuscript. All authors approve the final version to be published.

exogenous hydrogen peroxide supplementation partially rescued the ECM-inhibited osteoclastogenesis. Furthermore, rather than collagen type I, fibronectin in the ECM contributed to ECM-mediated anti-osteoclastogenesis. In conclusion, stem cell-derived decellularized ECM significantly suppressed osteoclastogenesis via the attenuation of intracellular ROS. The anti-osteoclastogenic property of cell-derived ECM may benefit its clinical use for modulating bone remodeling and promoting bone tissue engineering.

Graphical Abstract

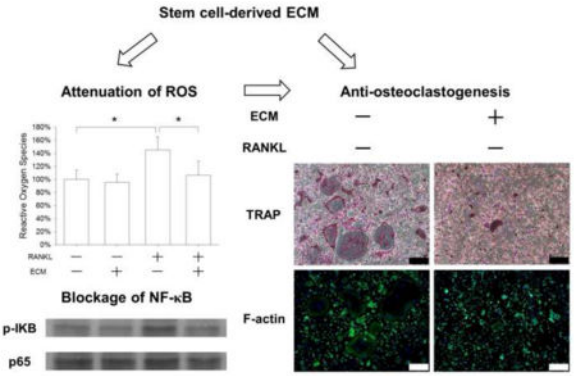

Keywords

extracellular matrix; bone marrow monocytes; osteoclasts; reactive oxygen species; NF-κB

1. Introduction

There is an increasing worldwide demand for suitable bone grafts to repair large bone defects in many clinical situations, such as trauma, tumor removal, or degenerative diseases. An optimal implant biomaterial is a key factor in bone tissue engineering, not only providing sufficient mechanical strength to support the body weight, but also facilitating new bone formation [1]. Autologous bone graft is currently regarded as the gold standard clinically because of its three-dimensional osteoconductive structure, the endogenous growth factors (e.g., bone morphogenetic proteins), and osteogenic precursor cells that respond to these signals [2]. However, bone site morbidity and size mismatch limit its clinical applications. At present, decellularized bone matrix attracts great interest in bone tissue engineering. Bone tissues can be obtained from allogenic or xenogenic donors and, after removing the original cells, most of the native extracellular matrix (ECM) proteins and the intact mechanical structure are preserved [3]. It has been reported that decellularized bone matrix promoted osteogenesis of mesenchymal stem cells (MSCs) *in vitro* [4] and repaired critical-sized calvarial defects *in vivo* [5]. However, the limited resources of human bone tissue, potential risk of disease transmission of allogenic tissues, and immunogenicity of ECM materials are still obstacles to their clinical use.

Recently, it has been demonstrated that stem cell-derived ECM is a promising biomaterial candidate for bone tissue engineering that facilitates large-scale expansion of MSCs *in vitro* while maintaining MSC phenotypes. The ECM is largely composed of collagens and various

types of matrix components, such as fibrillins, fibulins, fibronectin (FN), elastin, and biglycans [6], similar to the organic phase of bone tissue. More importantly, cell-derived ECM has been shown to enhance the lineage-specific differentiation of MSCs. Previous studies from our laboratory demonstrated that decellularized cell-derived ECM promoted *in vitro* osteogenic [7], chondrogenic [8], and hepatic [9] differentiation of bone marrow MSCs and successfully repaired *in vivo* partial-thickness cartilage defects in minipigs [10]. Interestingly, ECM deposited by fetal synovium MSCs has been shown to restore proliferation and chondrogenic potential of adult MSCs [6]. In addition, cell-derived ECM increased the levels of intracellular antioxidant enzymes in MSCs [11, 12] and improved the MSCs' resistance to oxidative stress-induced premature senescence through activating the silent information regulator type 1 (SIRT1)-dependent signaling pathway [13]. In bone tissue engineering, it has been reported that the ECM greatly enhanced the osteoinductive properties of three-dimensional synthetic polymer-based scaffolds by supporting osteoblastic differentiation of MSCs and accelerating matrix mineralization [14].

Bone regeneration is a complex process involving not only bone formation but also bone resorption. Osteoblasts control the formation and mineralization of new bone tissue by producing collagenous and non-collagenous ECM proteins. Osteoclasts are bone-resorbing cells that play a crucial role in bone remodeling by degrading both inorganic and organic bone components. These cells originate from the monocyte/macrophage lineage of hematopoietic precursors in bone marrow and are formed by the fusion of mononucleated progenitors [15]. Macrophage-colony stimulating factor (M-CSF) and receptor activator of nuclear factor-κB ligand (RANKL) are the two key cytokines essential for the osteoclastogenesis of bone marrow monocytes (BMMs). After binding with their membrane receptors, these cytokines activate several intracellular signaling pathways, such as the nuclear factor κ-light-chain-enhancer of activated B cells (NF-κB), to induce BMMs to differentiate toward the osteoclast lineage. During osteoclastic development, it has been observed that tartrate-resistant acid phosphatase (TRAP) is highly expressed in osteoclasts and thus TRAP staining is commonly used to differentiate osteoclasts and undifferentiated monocytes [16]. Before starting resorption activity, a podosome belt is formed in multinucleated osteoclasts, which is composed of integrins, F-actin, vinculin, adhesion proteins, and signaling proteins [17]. The actin rings are unique properties of active osteoclasts and their appearance is usually used as a typical marker for osteoclasts. Cathepsin K (CTSK) is another marker for osteoclasts that is secreted by mature osteoclasts to degrade collagens in bone matrix [18].

Besides their resorption activity, osteoclasts are important for bone remodeling by affecting bone formation. Interleukin-1 (IL-1) has been shown to support osteoclast differentiation by an autocrine mechanism [19] and to inhibit osteogenic differentiation of MSCs [20]. However, it was suggested that anabolic factors, secreted by osteoclasts, induced *in vitro* bone nodule formation [21] and Matsuoka *et al.* recently showed that osteoclast-derived complement component 3a promoted osteoblast differentiation [22]. On the other hand, osteoblasts have been proven to effectively influence osteoclast formation. Osteoprotegerin (OPG), released from osteoblasts, can inhibit osteoclast differentiation by interfering with the binding between RANKL and its membrane receptors [23]. Furthermore, the stimulating effect of cytokines on osteoclast differentiation is modulated by the cell-matrix interaction,

possibly because the factors can be stored in the bone matrix and released from the resorbed matrix by enzymatic cleavage [24]. Therefore, cell-derived ECM has been shown to support osteoblast differentiation and bone formation; however, the effect of this ECM on osteoclast differentiation and bone resorption remains unknown. Meanwhile, the underlying molecular mechanisms by which cell-derived ECM modulates the osteoclastogenesis of BMMs needs to be fully elucidated.

In this study, primary BMMs were isolated from the femurs and tibias of C57BL/6 mice and cell-derived ECM was produced by bone marrow MSCs (BM-MSCs). To evaluate the effect of the cell-derived ECM on osteoclast differentiation, BMMs were cultured on the ECM and standard tissue culture polystyrene (TCPS), and then induced toward osteoclasts *in vitro*. In addition, to identify the role of matrix protein components on osteoclastogenesis, BMMs were cultured on TCPS, COL I-coated, FN-coated, and ECM-coated substrates and osteoclast differentiation was evaluated. The underlying molecular mechanisms involving the NF-κB signaling pathway and intracellular reactive oxygen species (ROS) in the osteoclast precursors were investigated.

2. Materials and methods

2.1. Animals, reagents, and antibodies

Adult male C57BL/6 mice were purchased from Suzhou Healthytech Bio-pharmaceutical Co., Ltd. (Suzhou, China). Mouse bone marrow MSCs were obtained from Cyagen Biosciences Inc. (Guangzhou, China). Standard TCPS plates and dishes were purchased from Costar (Tewksbury, MA, USA). M-CSF and RANKL were purchased from PeproTech (Rocky Hill, NJ, USA). Fetal bovine serum (FBS), alpha minimum essential medium (α-MEM), penicillin, streptomycin, FN, 4′,6-diamidino-2-phenylindole (DAPI), and TRIzol® reagent were purchased from Thermo Fisher Scientific (Waltham, MA, USA). Gelatin, glutaraldehyde, ethanolamine, L-ascorbic acid, phosphate buffered saline (PBS), Triton X-100, NH_4OH, DNase I, COL I, hydrogen peroxide (H_2O_2), paraformaldehyde, bovine serum albumin (BSA), Triton X-100, and 2′,7′-dichlorofluorescein diacetate ($DCFH_2$-DA) were obtained from Sigma-Aldrich (St. Louis, MO, USA). All primary antibodies were purchased from Abcam (Cambridge, MA, USA).

2.2. Preparation of stem cell-derived ECM

Cell culture plates were treated with 0.2% gelatin for 1 h at 37°C, followed by 1% glutaraldehyde and 1 M ethanolamine for 30 min at room temperature. Mouse BM-MSCs were seeded onto the pretreated surface in a standard growth medium (α-MEM supplemented with 10% FBS, 100 U/mL of penicillin, and 100 μg/mL of streptomycin) at 37°C in a 5% CO_2 incubator and, after the cells reached 90% confluence, 100 μM of L-ascorbic acid was added for an additional 8 days. To remove the ECM-producing cells, matrix was treated with PBS containing 0.5% Triton X-100 and 20 mM NH_4OH (pH = 7.4) for 5 min, and subsequently treated with 100 U/mL DNase I for 1 h at 37°C. Decellularized cell-derived ECM was washed with PBS three times and stored under sterile conditions at 4°C.

2.3. Isolation and culture of primary monocytes from mouse bone marrow

BMMs were isolated from C57BL/6 mice as previously described [25]. The femurs and tibias were obtained aseptically and, after cutting off the ends of the bones, marrow cells were flushed out using a sterile syringe and saline. To remove red blood cells, the marrow cells were treated with red blood cell lysis buffer (Beyotime Institute of Biotechnology, Haimen, China) following the manufacturer's instructions. After washing, the cells were cultured in the standard growth medium at 37°C with 5% CO_2 in 60-mm cell culture dishes. To remove bone marrow stromal/mesenchymal cells, suspended cells were collected on the second day and re-cultured in the standard growth medium supplemented with 100 ng/mL M-CSF. After a three-day culture, non-adherent lymphocytes were removed by medium change. The cell morphology of BMMs was observed using a Zeiss Axiovert 40 CFL phase contrast microscope (Carl Zeiss Ltd., Oberkochen, Germany).

2.4. Flow cytometric analysis

Monocytes (n = 3) of each 1×10^6 cells were incubated in PBS containing 1% BSA and 1% NaN_3 (Sigma) on ice for 30 min. The cells were incubated in appropriately diluted mouse monoclonal antibodies against CD11b for 30 min and, after washing with PBS, cells were incubated with the secondary antibody (phycoerythrin–conjugated donkey anti-mouse IgG, Abcam) for another 30 min in the dark. Negative controls received equivalent amounts of isotype-matched antibodies (Abcam). Cells were measured using a Cytomics FC500 Flow Cytometer (Beckman-Coulter, Brea, CA, USA) and 10,000 events from each cell sample were analyzed using the WinMDI (Windows Multiple Document Interface for Flow Cytometry) 2.9 software.

2.5. Cell proliferation

Cell proliferation of BMMs was evaluated using a Quant-iT™ PicoGreen® dsDNA Assay Kit (Thermo Fisher Scientific). The cells were lysed by treating with 125 μg/mL papain lysis buffer for 4 h at 60°C. Equal quantities of lysates and reagent were added to a 96-well plate and then incubated in the dark for 5 min. The fluorescence values were measured using a SynergyMx multi-mode microplate reader (BioTek, Winooski, VT, USA) with an excitation wavelength of 485 nm and an emission wavelength of 520 nm alongside a standard curve.

2.6. Scanning electron microscopy (SEM) analysis

TCPS-cultured and ECM-cultured BMMs were fixed in 2.5% glutaraldehyde for 2 h and dehydrated in graded ethanol change (50%, 75%, 80%, 95%, and 100% ethanol concentration). The samples were dried using an automated critical point dryer (CPD300; Leica, Vienna, Austria) and subsequently sputter-coated with gold (SC7620; Quorum Technologies, Lewes, UK). The morphology of BMMs was analyzed by SEM (Quanta 250, FEI, Hillsboro, OR, USA) using a magnification of 2000×.

2.7. *In vitro* osteoclast differentiation

BMMs were cultured on TCPS or ECM and induced toward osteoclasts by incubating with standard growth medium supplemented with 20 ng/mL M-CSF and RANKL ranging from 25 to 100 ng/mL. To evaluate the role of ECM protein components in modulating

osteoclastogenesis, TCPS plates were pre-coated separately with COL I and FN. COL I was dissolved in 20 mM acetic acid and coated on the TCPS surface (10 μg/cm^2) at 4°C overnight and FN was coated on the TCPS surface (1 μg/cm^2) for 1 h at 37°C. BMMs were plated on different substrates (TCPS, COL I, FN, and ECM) and induced toward osteoclasts by treatment with 20 ng/mL M-CSF and 50 ng/mL RANKL. Cells were cultured for 5 days and the culture media was changed every other day.

2.8. TRAP staining

Osteoclasts cultured on TCPS and ECM were staining using a Leukocyte Acid Phosphatase Kit (Sigma-Aldrich) as previously described [26]. The cells were fixed with 4% paraformaldehyde for 15 min. After washing with deionized water, the fixed cells were incubated in acetate buffered solution containing naphthol AS-BI phosphate and tartrate solution (0.335 mol/L) at 37°C and then counterstained with DAPI. Osteoclast differentiation was determined by counting the number of multinucleated (≥ 3 nuclei or ≥ 8 nuclei) TRAP-positive cells in ten randomly chosen fields of view (FOV) using an Olympus IX51 microscope (Olympus Corporation, Tokyo, Japan).

2.9. Immunofluorescence staining

Osteoclasts cultured on TCPS and ECM were fixed with 4% paraformaldehyde for 15 min at room temperature. F-actin rings were stained with CytoPainter Phalloidin-iFluor 488 Reagent (Abcam) for 1 h according to the manufacturer's instructions. Cell nuclei were counterstained with DAPI. Immunofluorescence images of F-actin rings were captured by an Olympus IX51 microscope. Using the ImageJ software (National Institutes of Health, Bethesda, MD, USA), at least 20 multinucleated osteoclasts in 10 randomly chosen fields were analyzed for the areas of F-actin rings. The number of nuclei within F-actin rings and total nuclei in all cells was quantified. The percent nuclei in F-actin was expressed as an index for fusion efficiency, which was calculated as nuclei within F-actin rings divided by total nuclei [25].

To investigate the role of NF-κB in osteoclastogenesis, osteoclasts were first fixed in ice-cold methanol for 15 min and then permeabilized for 5 min in 0.1% Triton X-100. The cells were blocked for 30 min with 1% BSA and incubated in appropriately diluted primary antibodies against p65 for 1 h. After a brief washing with PBS, an Alexa Fluor® 488 donkey anti-mouse IgG secondary antibody (Thermo Fisher Scientific) was used. Cell nuclei were stained with DAPI for 5 min. Fluorescence images were obtained using an Olympus IX51 microscope.

2.10. Measurement of intracellular ROS

BMMs were first detached from TCPS or ECM and then incubated in α-MEM containing 50 μM $DCFH_2$-DA for 30 min at 37°C. The fluorescence intensity was measured using a Cytomics FC500 Flow Cytometer and 10,000 events from each cell sample were analyzed using the WinMDI (Windows Multiple Document Interface for Flow Cytometry) 2.9 software.

2.11. Total RNA extraction and real-time reverse transcription-polymerase chain reaction (real-time RT-PCR)

Total RNA was extracted using the TRIzol® reagent and 500 ng RNA were reverse-transcribed using the RevertAid First Strand cDNA Synthesis Kit (Thermo Fisher Scientific). Quantitative real-time RT-PCR assays were performed using a CFX96™ Real-Time RT-PCR System (Bio-Rad, Hercules, CA, USA) and the iTap™ Universal SYBR® Green Supermix kit (Bio-Rad). The expression of the following genes was analyzed: *TRAP*, *CTSK*, and osteoclast-associated receptor (*OSCAR*). Glyceraldehyde-3-phosphate dehydrogenase (*GAPDH*) was used as housekeeping reference gene. All applied primer sequences are listed in Table 1. Relative transcript levels were calculated using the ΔΔCt method [26] and were expressed in fold change compared to an undifferentiated or the TCPS control.

2.12. Western blot analysis

Osteoclasts cultured on TCPS and ECM were collected and protein was extracted by ice-cold cell lysis buffer (Beyotime) containing protease inhibitors (Thermo Fisher Scientific). The protein concentration was measured using a BCA protein assay kit (Beyotime). Heat-denatured protein samples were separated by polyacrylamide gel electrophoresis (Beyotime) and then transferred onto nitrocellulose membranes (Thermo Fisher Scientific). After blocking with 5% non-fat dry milk for 1 h, the membranes were incubated with primary antibodies against IκB-α (phospho S32), IκB-α, p65, and GAPDH overnight at 4°C. Subsequently, the membranes were incubated with horseradish peroxidase-conjugated goat anti-mouse IgG (H +L) and anti-rabbit IgG (H +L)-labeled secondary antibodies (Thermo Fisher Scientific). Specific immune complexes were visualized on a CL-XPosure Film (Thermo Fisher Scientific) using SuperSignal West Pico Substrate (Thermo Fisher Scientific) following the manufacturer's instructions. The levels of each protein were compared after normalization against GAPDH as an internal control using the ImageJ software.

2.13. Statistical analysis

All data were analyzed using the SPSS 13.0 statistical software (SPSS Inc., Chicago, IL, USA) and were expressed as means ± standard error of mean (S.E.M.). Statistical differences were determined using the two-tailed Student's *t*-test and the analysis of variance with a Tukey's post hoc test for multiple group comparisons. Significance was indicated by a p-value < 0.05 (*) or < 0.01 (**).

3. Results

3.1. Identification of BMMs isolated from C57BL/6 mice

We examined the cellular properties of BMMs isolated from the femurs and tibias of C57BL/6 mice. BMMs were seeded at the initial density of 3,000 cells/cm^2 and treated with 20 ng/mL M-CSF for 96 h. BMMs showed a small and round morphology with increased cell density (Fig. 1A). Flow cytometry data showed that BMMs strongly expressed CD11b (97.7 ± 0.4%), which is a typical biomarker of the monocyte/macrophage lineage (Fig. 1B).

To determine their osteoclast formation potential, an *in vitro* osteoclastogenesis of BMMs was performed by treating them with 20 ng/mL M-CSF and 50 ng/mL RANKL. After a 5-day culture, multinucleated and TRAP-positive osteoclasts were observed in the RANKL-treated group whereas, in the absence of RANKL, BMMs failed to differentiate into mature osteoclasts. The functional morphology of osteoclasts was further assessed using immunofluorescence staining with phalloidin. In the presence of RANKL, multinucleated osteoclasts with a full actin ring were observed (Fig. 1C). The transcript levels of osteoclast-specific genes in the RANKL-treated BMMs were significantly up-regulated, including *TRAP* (Fig. 1D), *CTSK* (Fig. 1E), and *OSCAR* (Fig. 1F).

3.2. Cell-derived ECM promotes cell proliferation of BMMs

BMMs were cultured on standard TCPS and cell-derived ECM and treated with 20 ng/mL M-CSF. Both BMMs showed similar cell morphology (Fig. 2A), but the cell proliferation of the ECM group was significantly higher than the TCPS group (Fig 2B). In the presence of M-CSF, cell proliferation of the ECM-cultured BMMs was 59.2% and 35.4% higher than those on TCPS on Days 5 and 7, respectively. Flow cytometry data showed that there was no significant difference between the expression of CD11b in TCPS-cultured and ECM-cultured BMMs (96.3 ± 1.5% vs. 96.6 ± 2.1%) (Fig. 2C). The SEM images showed that the cell morphology of the ECM-cultured and the TCPS-cultured BMMs was similar, but the TCPS-cultured cells were more flattened (Fig. 2D).

3.3. Cell-derived ECM inhibits osteoclast differentiation of BMMs

BMMs were cultured on standard TCPS and cell-derived ECM and induced toward osteoclasts in the presence of RANKL at the concentration of 25, 50, or 100 ng/mL. When BMMs were cultured on TCPS, treatments with RANKL induced TRAP-positive multinucleated osteoclasts in a dose-dependent manner; however, osteoclast formation was inhibited when culturing on cell-derived ECM (Fig. 3A). Quantitative results showed that the number of TRAP-positive osteoclasts with greater than 3 nuclei in the TCPS group was significantly more than the ECM group after treatments with RANKL (7.4 ± 2.6 vs. 2.5 ± 1.1 at 25 ng/mL, 19.8 ± 2.4 vs. 7.0 ± 1.7 at 50 ng/mL, and 20.9 ± 3.3 vs. 11.1 ± 1.9 at 100 ng/mL) (Fig. 3B). Similarly, the number of TRAP-positive osteoclasts with 8 or more nuclei in the ECM group was significantly fewer than in the TCPS group (Fig. 3C). When culturing on TCPS, the transcript levels of *TRAP* mRNA in RANKL-treated BMMs were significantly higher than those on ECM (by 22.1% at 25 ng/mL, 66.1% at 50 ng/mL, and 72.3% at 100 ng/mL) (Fig. 3D). In the presence of 100 ng/mL RANKL, the mRNA expression of *CTSK* (Fig. 3E) and *OSCAR* (Fig. 3F) were 3.0-fold and 5.4-fold, respectively, more in the TCPS-cultured BMMs than those on the ECM.

The immunofluorescence staining assay revealed that the formation of actin rings in multinucleated osteoclasts was also inhibited by cell-derived ECM (Fig. 4A). In the presence of 25 ng/mL RANKL, no multinucleated osteoclast formation was observed in the ECM group. The average F-actin ring areas of TCPS-cultured osteoclasts were 29.7-fold at 50 ng/mL and 24.7-fold at 100 ng/mL compared with those on the ECM (Fig. 4B). In addition, the percentage of nuclei in F-actin rings was expressed as an index for fusion efficiency and quantitative results showed the fusion efficiency was significantly higher in the TCPS group

(24.3 ± 3.5% vs. 4.7 ± 1.6% at 50 ng/mL, and 37.0 ± 6.0% vs. 4.8 ± 1.3% at 100 ng/mL) (Fig. 4C).

3.4. The role of ECM components in modulating osteoclastogenesis

To evaluate the different effects of ECM protein components on osteoclast formation, BMMs were induced toward osteoclasts on four substrates: uncoated TCPS, COL I, FN, or ECM. The TRAP staining results confirmed that, after a 5-day osteoclastogenic induction, the formation of multinucleated osteoclasts and F-actin rings was observed in the TCPS and COL I groups (Fig. 5A); however, quantitative analysis revealed that the number of TRAP-positive osteoclasts with greater than 3 nuclei in the FN and ECM groups was significantly reduced (22.8 ± 3.4 on TCPS, 19.7 ± 2.5 on COL I, 16.3 ± 3.9 on FN, and 7.0 ± 1.6 on ECM) (Fig. 5B). Similarly, the number of TRAP-positive osteoclasts with 8 or more nuclei in the FN and ECM groups was also significantly decreased compared with the TCPS and COL I groups (Fig. 5C). The immunofluorescence staining results showed that multinucleated osteoclasts with a full actin ring were observed on the substrates of TCPS, COL I, and FN (Fig. 5A). The average F-actin ring area was decreased by 39.7% on COL I, by 76.9% on FN, and by 96.9% on ECM, compared to the cells cultured on TCPS (Fig. 5D). The percentage of nuclei in F-actin was significantly lower in the FN and ECM groups compared with the TCPS group, suggesting decreased fusion events in FN and ECM cultures (Fig. 5E). Similarly, the real-time RT-PCR data showed that the transcript levels of osteoclast-specific genes were significantly lower in the FN and ECM groups. When culturing on the FN substrate, the mRNA expression was decreased by 41.1% (*TRAP* mRNA, Fig. 5F), by 38.5% (*CTSK* mRNA, Fig. 5G), and by 50.3% (*OSCAR* mRNA, Fig. 5H), compared to the levels in the TCPS-cultured osteoclasts.

3.5. Molecular mechanisms of ECM-mediated anti-osteoclastogenesis

To investigate the underlying molecular mechanisms involved in ECM-mediated inhibition of osteoclastogenesis, we measured the intracellular ROS levels. In the absence of RANKL, cell-derived ECM showed no effect on ROS production; however, in the presence of 50 ng/mL RANKL, the ROS level of ECM-cultured BMMs was decreased by 26.6% compared with the TCPS group (Fig. 6A). Furthermore, we evaluated the effect of ECM on the NF-κB signaling pathway during osteoclastogenesis. When BMMs were cultured on TCPS, RANKL treatment resulted in nuclear translocation of p65, a marker of NF-κB activation, from the cytoplasm into the nucleus. However, the translocation of p65 was inhibited in the ECM-cultured cells, suggesting that the NF-κB signaling pathway was blocked by the ECM substrate (Fig. 6B). The western blot results showed that the phosphorylation of IκB in RANKL-treated BMMs was attenuated by cell-derived ECM (Fig. 6C), and the protein level of p65 in ECM-cultured BMMs was decreased as well (Fig. 6D).

3.6. Supplementation with exogenous hydrogen peroxide restores ECM-inhibited osteoclastogenesis

To confirm whether ECM inhibited osteoclast differentiation of BMMs via the intracellular ROS pathway, BMMs were induced toward osteoclasts with or without the addition of 20 μM H_2O_2. The TRAP staining assay showed that H_2O_2 treatment increased the number of TRAP-positive osteoclasts, even when cells were cultured on ECM (Fig. 7A). The

quantitative results demonstrated that, when culturing on cell-derived ECM, H_2O_2 treatment increased the number of TRAP-positive osteoclasts with greater than 3 nuclei by 68.5% (Fig. 7B) and resulted in a 3.6-fold increase in the number of TRAP-positive osteoclasts with 8 or more nuclei (Fig. 7C). The transcript level of *TRAP* was up-regulated by 65.8% and 134.9% by H_2O_2 treatment in the TCPS-cultured and ECM-cultured BMMs, respectively (Fig. 7D). The mRNA expression of *CTSK* (Fig. 7E) was increased by 76.0% and the mRNA level of *OSCAR* (Fig. 7F) was up-regulated by 41.4% in the ECM-cultured cells. These results suggest that exogenous H_2O_2 treatment partly restored ECM-inhibited osteoclastogenesis of BMMs.

Furthermore, we found that H_2O_2 treatment significantly increased the level of intracellular ROS by 22.9% in the TCPS-cultured BMMs and 58.5% in the ECM-cultured BMMs (Fig. 8A). Immunofluorescence staining assay revealed that H_2O_2 treatment promoted the nuclear translocation of p65 in some ECM-cultured BMMs (Fig. 8B). The western blot assay confirmed that H_2O_2 treatment up-regulated the phosphorylated level of IκB and the protein expression of p65 in the ECM-cultured BMMs. These results indicated that exogenous supplementation with H_2O_2 activated the ECM-inhibited NF-κB signaling pathway during osteoclast differentiation.

4. Discussion

Cell-derived ECM is a promising biomaterial for bone tissue engineering. After decellularization, this cell-derived ECM maintains the original three-dimensional structure and matrix components [7]. It has been shown that decellularized ECM enhanced the biological performance of plain synthetic polymer scaffolds by promoting osteogenic differentiation of human MSCs [14]; however, the effect of decellularized ECM on osteoclast differentiation is unknown. Wear particles from bone implant materials usually induce cytokine release from surrounding inflammatory cells [27] and these pro-inflammatory cytokines further activate osteoclasts to dissolve the new bone matrix and affect the quality of bone healing around implants. Therefore, we studied the osteoclastogenesis of BMMs and osteoclastic cell behavior on cell-derived ECM in this study; our results may benefit the design of new bone implants by combining with decellularized ECM to accelerate bone regeneration [28].

Previous studies have demonstrated that the resorption effect of osteoclasts on ECM networks impacts bone remodeling. Osteoclasts dissolve minerals in the resorption site by secreting hydrochloric acid and degrade the organic matrix by secreting proteases, such as cathepsin K. Our current study demonstrates that stem cell-derived decellularized ECM potently inhibits the osteoclastogenesis of primary BMMs. This inhibitory effect of cell-derived ECM on osteoclast differentiation has been confirmed by fewer TRAP-positive multinucleated cells, smaller areas of actin rings, and lower levels of osteoclast-specific gene expression. Even in the presence of RANKL at a high concentration (100 ng/mL), monocytes on ECM still failed to differentiate toward functional osteoclasts, while RANKL at low concentrations, such as 25 ng/mL, was sufficient to induce BMMs to form multinucleated osteoclasts on standard TCPS. In a recent study, it was shown that ECM proteins (fibronectin, vitronectin, and osteopontin) modulated osteoclast morphologies

between compact, spread, and migratory shapes, indicating that bone matrix proteins were essential for osteoclast resorption activity [29]. Kajahn *et al.* synthesized artificial ECMs composed of type I collagen and sulfated hyaluronan, and found that the differentiation of monocytes into inflammatory M1 macrophages was inhibited and the secretion of pro-inflammatory cytokines was reduced [30]. Since osteoporosis is characterized by abnormal bone resorption, the anti-osteoclastogenic effect of ECM could contribute to a potential bone graft that can benefit bone fracture healing in osteoporotic patients by suppressing osteoclast activity.

To explore the underlying mechanisms by which cell-derived ECM inhibits the osteoclastogenesis of BMMs, we compared the roles of two important matrix proteins, COL I and FN, in the process of osteoclast differentiation. Based on our previous work, these two proteins are abundant in cell-derived ECM and, even after decellularization, they are mostly preserved in the ECM [7]. Surprisingly, BMMs cultured on the FN-coated substrate showed weaker osteoclast differentiation, while the formation of large multinucleated osteoclasts and the transcript levels of osteoclast-specific genes were barely affected by the COL I-coated substrate, suggesting that FN was at least partially responsible for ECM-mediated anti-osteoclastogenesis. Consistent with our findings, Gramoun *et al.* evaluated the effect of fibronectin on two osteoclast precursor cells, RAW 264.7 cells and mouse splenocytes. They demonstrated that fibronectin inhibited osteoclastogenesis by directly delaying osteoclast fusion by up-regulating nitric oxide levels [31]. Meanwhile, the role of COL I in cell-derived ECM is dependent on different cell types. COL I showed no effect on osteoclast differentiation in this study, but in a recent study from our laboratory, COL I has been suggested to play an important role in preventing oxidative stress-induced premature senescence in MSCs [13]. Furthermore, it has been shown that during inflammatory conditions, collagen facilitated maturation of monocyte-derived dendritic cells through the OSCAR-mediated signaling pathway [32].

In addition, other matrix components in cell-derived ECM may contribute to the inhibition of osteoclastogenesis of BMMs. Sulfated glycosaminoglycans (GAGs), which are the major components of bone ECM, have been shown to inhibit the differentiation and resorption functions of osteoclasts [33]. Another important matrix protein in bone, fibrillin-1, has been identified in cell-deposited ECM [6] and inhibits the osteoclastogenesis of bone marrow-derived precursors by interfering with the RANKL-mediated signaling pathway [34]. Furthermore, the mineralization of bone matrix is possibly a key factor that regulates osteoclast functions. A recent study from Pernelle *et al.* suggested that osteoclasts preferentially resorb cortical bone that has lower mineral content and weaker mechanical properties [35]. Osteoclastogenesis and osteoclast functions were enhanced on carbonated hydroxyapatite rather than hydroxyapatite or β-tricalcium phosphate, suggesting that the mineral phase in the ECM may regulate osteoclast differentiation differently [36]. The ECM used in this study was deposited by bone marrow-derived MSCs, so the effect of mineralized cell-derived ECM on osteoclast formation is unknown. In our future studies, a full characterization of stem cell-derived ECM using proteomics analyses will be necessary; it may help to elucidate other types of matrix components in the ECM that have a similar anti-osteoclastogenic effect. It would also be interesting to know whether matrix mineralization regulates osteoclast differentiation. The resorption activity of osteoclasts will also be

quantified by measuring the concentration of calcium ions in the culture medium when BMMs are induced toward osteoclasts on mineralized cell-derived ECM.

Osteoclast differentiation is initiated when autocrine or paracrine cytokines, such as M-CSF and RANKL, bind to their receptors and the intracellular NF-κB is subsequently activated. In this study, we found that RANKL treatment was sufficient to activate NF-κB in the TCPS-cultured BMMs but, when culturing on cell-derived ECM, the NF-κB signaling pathway was completely inactivated, as evidenced by the blockage of nuclear translocation of p65 and decreased phosphorylation of IκB. However, the effects of ECM on NF-κB activation depend on different cell types. For example, extracellular matrix derived from 804G cells rich in laminin-5 induces nuclear translocation and the DNA binding activity of p65 in pancreatic beta cells; this ECM-mediated NF-kB activity supports insulin secretion [37]. Another study demonstrated that chondrocyte-derived ECM not only inhibited NF-κB activation but also decreased the expression of pro-inflammatory cytokines in human pterygium epithelial cells [38]. Furthermore, the effect of ECM on osteoclast functions has been suggested to depend on receptor-ligand communication. Integrins are one of the most abundant receptors on monocytes and play an important role in osteoclast maturation. The resorption activity of osteoclasts was inhibited by a type II collagen N-propeptide through activation of the integrin $\alpha_v\beta_3$, while the reduction of the integrin levels by siRNA alleviated the inhibitory effect of the propeptide on osteoclast differentiation [39]. In contrast, the matrix adhesion protein ameloblastin was shown to enhance the osteoclastogenesis of BMMs via integrin $\alpha_2\beta_1$-mediated signal transduction [40]. In addition, Toll-like receptor 4 (TLR4) has been suggested as another important mediator in regulating bone remodeling, which mediated the inhibitory effect of hyaluronan on osteoclast differentiation [41].

The importance of RANKL-induced ROS production in modulating osteoclast differentiation is well established. RANKL stimulation induces a significant increase in intracellular ROS in BMMs through activating tumor necrosis factor receptor-associated factor (TRAF) 6 and nicotinamide adenine dinucleotide phosphate oxidase (Nox) 1. The intracellular ROS acts as a crucial signal mediator for osteoclastogenesis, because supplementation with an antioxidant, N-acetylcysteine (NAC), abolishes both RANKL-mediated ROS production and osteoclast differentiation [42]. In this study, we observed that the intracellular ROS level in the TCPS-cultured BMMs, but not the ECM-cultured BMMs, was up-regulated by RANKL treatment. We speculated that the decreased level of ROS production in the ECM-cultured BMMs contributed to the subsequent inhibition of osteoclastogenesis. The reduction of intracellular ROS production by cell-derived ECM was possibly due to the enhanced levels of intracellular antioxidant enzymes, such as catalase, superoxide dismutase, and glutathione peroxidase 1 [11]. Nuclear factor-erythroid 2-related factor 2 (Nrf2) is possibly involved in ROS production, which functions as a redox-sensitive transcription factor by regulating the expression of antioxidant and detoxification genes. In Nrf2-deficient osteoclast precursor cells, the intracellular ROS level was significantly increased and RANKL-induced osteoclastogenesis was substantially promoted [43]. To further investigate the role of ROS production in ECM-mediated inhibition of osteoclast differentiation, we treated the ECM-cultured BMMs with exogenous H_2O_2 in addition to RANKL stimulation. Our results showed that the inhibitory effect of decellularized ECM on osteoclastogenesis was partially counteracted, as indicated by the increased levels of ROS

production, nuclear translocation of p65, and up-regulated transcript levels of osteoclast-specific genes. In agreement with our results, Lean *et al.* showed that H_2O_2 is an essential regulator responsible for osteoclast formation and bone resorption, which was abolished by the over-expression of glutathione peroxidase 1, a primary intracellular antioxidant enzyme that degrades H_2O_2 [44]. Similarly, a recent report has shown that inhibition of ROS production by antioxidant treatments, such as coenzyme Q10, selenite, and curcumin, are effective in suppressing osteoclast formation [45]. Therefore, targeting the intracellular ROS may represent a potential therapeutic approach to preventing bone resorption and treating disordered bone metabolism. Future experiments are necessary to identify the specific types of intracellular ROS and to clarify the detailed signaling transduction pathways in ECM-mediated anti-osteoclastogenesis.

In addition to the direct inhibitory effect on osteoclast differentiation, the promotion of osteogenesis and matrix mineralization in BM-MSCs by cell-derived ECM has been reported in a number of previous studies [13, 46]. Hence, we speculate that there might be other intracellular molecules or signaling pathways responsible for ECM-mediated anti-osteoclastogenesis, such as OPG, transforming growth factor β (TGF-β), insulin-like growth factor (IGF), and platelet-derived growth factor. For instance, OPG, a soluble decoy receptor for RANKL secreted by osteoblasts, has been shown to inhibit RANKL-induced osteoclast differentiation and bone resorption [47]. Sulfated GAGs were shown to improve osteoblast differentiation and concurrently suppress the paracrine support of osteoclast differentiation by up-regulating the expression of OPG [48]. Therefore, our future work will focus on the impact of cell-derived ECM on the expression of OPG and RANKL in osteoblasts. Furthermore, ECM-cultured BM-MSCs were shown to enhance the intracellular TGF-β1 signaling pathway [8], but the effect of TGF-β on osteoclast differentiation is still controversial. It was reported that TGF-β directly stimulated osteoclast differentiation from hematopoietic lineage cells [49], but Houde *et al.* [50] demonstrated that TGF-β inhibited the resorption activity of osteoclasts by inducing apoptosis. The effect of decellularized ECM on TGF-β expression in osteoblasts and whether ECM-mediated anti-osteoclastogenesis is dependent on TGF-β will be elucidated in our future studies.

However, this study was limited to *in vitro* observations, so animal studies will be necessary to confirm the anti-osteoclastogenic effect of stem cell-derived ECM *in vivo*. Previous studies have tested the applicability of using the decellularized ECM as a cell culture substrate to provide high-quality cells. Yang *et al.* showed that chondrocytes expanded on stem cell-derived ECM exhibited superior chondrocytic phenotype and that *in vivo* cartilage formation was confirmed after implanting subcutaneously for 14 days [51]. Furthermore, a potential therapeutic strategy of using stem cell-derived ECM is to generate biological bone implants by integrating the ECM with currently available scaffolds [52]. A functional bioactive material was investigated, in which decellularized stem cell-derived ECM was deposited on a biphasic calcium phosphate scaffold; this new biomaterial was shown to support MSC osteogenesis and bone formation [53]. Therefore, our future studies will produce bioactive implantable materials by combining stem cell-derived ECM with synthetic scaffolds that are similar to native bone tissue and to evaluate the effect of these ECM-scaffold biomaterials on *in vivo* bone formation and bone resorption.

5. Conclusions

Our study clearly demonstrates that stem cell-derived decellularized ECM suppresses the osteoclastogenesis of BMMs. Compared with cells on standard TCPS, the number of TRAP-positive multinucleated osteoclasts, the areas of actin rings, and the transcript levels of osteoclast-specific genes were significantly reduced in the ECM-cultured BMMs. The underlying molecular mechanisms involve blockage of the NF-κB signaling pathway and attenuation of intracellular ROS, evidenced by the fact that supplementation with exogenous H_2O_2 partially restores ECM-inhibited osteoclast differentiation. We also demonstrated that fibronectin, rather than collagen type I, contributes to the inhibitory effect of cell-derived ECM on osteoclastogenesis. The anti-osteoclastogenic property of cell-derived ECM may be beneficial clinically for modulating bone remodeling. By facilitating bone formation and inhibiting bone resorption, stem cell-derived decellularized ECM provides a new strategy to promote bone tissue engineering.

Acknowledgments

The authors are grateful to Suzanne Danley (West Virginia University, USA) and Jessica He (University of Waterloo, Canada) for carefully reviewing and editing the manuscript. This work was supported by the National Natural Science Foundation of China [31570978, 31771063, 81702146, 81401768, 11572211]; the Natural Science Foundation of Jiangsu Province [BK20140323, BK20140289]; the National Institutes of Health (NIH) [AR067747-01A1] and an Established Investigator Grant from the Musculoskeletal Transplant Foundation (MTF) to M.P.; and the Priority Academic Program Development of Jiangsu Higher Education Institutions (PAPD).

References

1. Yu X, Tang X, Gohil SV, Laurencin CT. Biomaterials for Bone Regenerative Engineering. Adv Healthc Mater. 2015; 4(9):1268–1285. [PubMed: 25846250]
2. Pape HC, Evans A, Kobbe P. Autologous bone graft: properties and techniques. J Orthop Trauma. 2010; 24(Suppl 1):S36–S40. [PubMed: 20182233]
3. Benders KE, van Weeren PR, Badylak SF, Saris DB, Dhert WJ, Malda J. Extracellular matrix scaffolds for cartilage and bone regeneration. Trends Biotechnol. 2013; 31(3):169–176. [PubMed: 23298610]
4. Hashimoto Y, Funamoto S, Kimura T, Nam K, Fujisato T, Kishida A. The effect of decellularized bone/bone marrow produced by high-hydrostatic pressurization on the osteogenic differentiation of mesenchymal stem cells. Biomaterials. 2011; 32(29):7060–7067. [PubMed: 21724252]
5. Lee DJ, Diachina S, Lee YT, Zhao L, Zou R, Tang N, Han H, Chen X, Ko CC. Decellularized bone matrix grafts for calvaria regeneration. J Tissue Eng. 2016; 7:2041731416680306. [PubMed: 28228929]
6. Li J, Hansen KC, Zhang Y, Dong C, Dinu CZ, Dzieciatkowska M, Pei M. Rejuvenation of chondrogenic potential in a young stem cell microenvironment. Biomaterials. 2014; 35(2):642–653. [PubMed: 24148243]
7. He F, Liu X, Xiong K, Chen S, Zhou L, Cui W, Pan G, Luo ZP, Pei M, Gong Y. Extracellular matrix modulates the biological effects of melatonin in mesenchymal stem cells. J Endocrinol. 2014; 223(2):167–180. [PubMed: 25210047]
8. Pei M, He F, Kish VL. Expansion on extracellular matrix deposited by human bone marrow stromal cells facilitates stem cell proliferation and tissue-specific lineage potential. Tissue Eng Part A. 2011; 17(23–24):3067–3076. [PubMed: 21740327]
9. He H, Liu X, Peng L, Gao Z, Ye Y, Su Y, Zhao Q, Wang K, Gong Y, He F. Promotion of hepatic differentiation of bone marrow mesenchymal stem cells on decellularized cell-deposited extracellular matrix. Biomed Res Int. 2013; 2013:406871. [PubMed: 23991414]

10. Pei M, He F, Li J, Tidwell JE, Jones AC, McDonough EB. Repair of large animal partial-thickness cartilage defects through intraarticular injection of matrix-rejuvenated synovium-derived stem cells. Tissue Eng Part A. 2013; 19(9–10):1144–1154. [PubMed: 23216161]
11. Liu X, Zhou L, Chen X, Liu T, Pan G, Cui W, Li M, Luo Z, Pei M, Yang H, He F. Culturing on decellularized extracellular matrix enhances antioxidant properties of human umbilical cord-derived mesenchymal stem cells. Mater Sci Eng C Mater Biol Appl. 2016; 61:437–448. [PubMed: 26838870]
12. Pei M, Zhang Y, Li J, Chen D. Antioxidation of decellularized stem cell matrix promotes human synovium-derived stem cell-based chondrogenesis. Stem Cells Dev. 2013; 22(6):889–900. [PubMed: 23092115]
13. Zhou L, Chen X, Liu T, Zhu C, Si M, Jargstorf J, Li M, Pan G, Gong Y, Luo ZP, Yang H, Pei M, He F. SIRT1-dependent anti-senescence effects of cell-deposited matrix on human umbilical cord mesenchymal stem cells. J Tissue Eng Regen Med. 2017; doi: 10.1002/term.2422
14. Sadr N, Pippenger BE, Scherberich A, Wendt D, Mantero S, Martin I, Papadimitropoulos A. Enhancing the biological performance of synthetic polymeric materials by decoration with engineered, decellularized extracellular matrix. Biomaterials. 2012; 33(20):5085–5093. [PubMed: 22510434]
15. Cappariello A, Maurizi A, Veeriah V, Teti A. The Great Beauty of the osteoclast. Arch Biochem Biophys. 2014; 558:70–78. [PubMed: 24976175]
16. Halleen JM, Alatalo SL, Suominen H, Cheng S, Janckila AJ, Vaananen HK. Tartrate-resistant acid phosphatase 5b: a novel serum marker of bone resorption. J Bone Miner Res. 2000; 15(7):1337–1345. [PubMed: 10893682]
17. Lakkakorpi PT, Vaananen HK. Kinetics of the osteoclast cytoskeleton during the resorption cycle in vitro. J Bone Miner Res. 1991; 6(8):817–826. [PubMed: 1664645]
18. Saftig P, Hunziker E, Everts V, Jones S, Boyde A, Wehmeyer O, Suter A, von Figura K. Functions of cathepsin K in bone resorption. Lessons from cathepsin K deficient mice. Adv Exp Med Biol. 2000; 477:293–303. [PubMed: 10849757]
19. Yao Z, Xing L, Qin C, Schwarz EM, Boyce BF. Osteoclast precursor interaction with bone matrix induces osteoclast formation directly by an interleukin-1-mediated autocrine mechanism. J Biol Chem. 2008; 283(15):9917–9924. [PubMed: 18250170]
20. Liu X, Gong Y, Xiong K, Ye Y, Xiong Y, Zhuang Z, Luo Y, Jiang Q, He F. Melatonin mediates protective effects on inflammatory response induced by interleukin-1 beta in human mesenchymal stem cells. J Pineal Res. 2013; 55(1):14–25. [PubMed: 23488678]
21. Karsdal MA, Neutzsky-Wulff AV, Dziegiel MH, Christiansen C, Henriksen K. Osteoclasts secrete non-bone derived signals that induce bone formation. Biochem Biophys Res Commun. 2008; 366(2):483–488. [PubMed: 18068671]
22. Matsuoka K, Park KA, Ito M, Ikeda K, Takeshita S. Osteoclast-derived complement component 3a stimulates osteoblast differentiation. J Bone Miner Res. 2014; 29(7):1522–1530. [PubMed: 24470120]
23. Chen X, Wang Z, Duan N, Zhu G, Schwarz EM, Xie C. Osteoblast-osteoclast interactions. Connect Tissue Res. 2017:1–9.
24. Detsch R, Boccaccini AR. The role of osteoclasts in bone tissue engineering. J Tissue Eng Regen Med. 2015; 9(10):1133–1149. [PubMed: 24478169]
25. Leung R, Wang Y, Cuddy K, Sun C, Magalhaes J, Grynpas M, Glogauer M. Filamin A regulates monocyte migration through Rho small GTPases during osteoclastogenesis. J Bone Miner Res. 2010; 25(5):1077–1191. [PubMed: 19929439]
26. Zhou L, Chen X, Yan J, Li M, Liu T, Zhu C, Pan G, Guo Q, Yang H, Pei M, He F. Melatonin at pharmacological concentrations suppresses osteoclastogenesis via the attenuation of intracellular ROS. Osteoporos Int. 2017; 28(12):3325–3337. [PubMed: 28956094]
27. Dapunt U, Giese T, Lasitschka F, Reinders J, Lehner B, Kretzer JP, Ewerbeck V, Hansch GM. On the inflammatory response in metal-on-metal implants. J Transl Med. 2014; 12:74. [PubMed: 24650243]

28. Kim IG, Hwang MP, Du P, Ko J, Ha CW, Do SH, Park K. Bioactive cell-derived matrices combined with polymer mesh scaffold for osteogenesis and bone healing. Biomaterials. 2015; 50:75–86. [PubMed: 25736498]
29. Gramoun A, Goto T, Nordstrom T, Rotstein OD, Grinstein S, Heersche JN, Manolson MF. Bone matrix proteins and extracellular acidification: potential co-regulators of osteoclast morphology. J Cell Biochem. 2010; 111(2):350–361. [PubMed: 20506338]
30. Kajahn J, Franz S, Rueckert E, Forstreuter I, Hintze V, Moeller S, Simon JC. Artificial extracellular matrices composed of collagen I and high sulfated hyaluronan modulate monocyte to macrophage differentiation under conditions of sterile inflammation. Biomatter. 2012; 2(4):226–236. [PubMed: 23507888]
31. Gramoun A, Azizi N, Sodek J, Heersche JN, Nakchbandi I, Manolson MF. Fibronectin inhibits osteoclastogenesis while enhancing osteoclast activity via nitric oxide and interleukin-1beta-mediated signaling pathways. J Cell Biochem. 2010; 111(4):1020–1034. [PubMed: 20672308]
32. Schultz HS, Nitze LM, Zeuthen LH, Keller P, Gruhler A, Pass J, Chen J, Guo L, Fleetwood AJ, Hamilton JA, Berchtold MW, Panina S. Collagen induces maturation of human monocyte-derived dendritic cells by signaling through osteoclast-associated receptor. J Immunol. 2015; 194(7):3169–3179. [PubMed: 25725106]
33. Salbach J, Kliemt S, Rauner M, Rachner TD, Goettsch C, Kalkhof S, von Bergen M, Moller S, Schnabelrauch M, Hintze V, Scharnweber D, Hofbauer LC. The effect of the degree of sulfation of glycosaminoglycans on osteoclast function and signaling pathways. Biomaterials. 2012; 33(33): 8418–8429. [PubMed: 22954516]
34. Tiedemann K, Boraschi-Diaz I, Rajakumar I, Kaur J, Roughley P, Reinhardt DP, Komarova SV. Fibrillin-1 directly regulates osteoclast formation and function by a dual mechanism. J Cell Sci. 2013; 126(Pt 18):4187–4194. [PubMed: 24039232]
35. Pernelle K, Imbert L, Bosser C, Auregan JC, Cruel M, Ogier A, Jurdic P, Hoc T. Microscale mechanical and mineral heterogeneity of human cortical bone governs osteoclast activity. Bone. 2017; 94:42–49. [PubMed: 27725316]
36. Nakamura M, Hentunen T, Salonen J, Nagai A, Yamashita K. Characterization of bone mineral-resembling biomaterials for optimizing human osteoclast differentiation and resorption. J Biomed Mater Res A. 2013; 101(11):3141–51. [PubMed: 23554241]
37. Hammar EB, Irminger JC, Rickenbach K, Parnaud G, Ribaux P, Bosco D, Rouiller DG, Halban PA. Activation of NF-kappaB by extracellular matrix is involved in spreading and glucose-stimulated insulin secretion of pancreatic beta cells. J Biol Chem. 2005; 280(34):30630–30637. [PubMed: 15994334]
38. Lee H, Lee M, Lee Y, Choi S, Yang J. Chondrocyte-derived extracellular matrix suppresses pathogenesis of human pterygium epithelial cells by blocking the NF-kappaB signaling pathways. Mol Vis. 2016; 22:1490–1502. [PubMed: 28050122]
39. Hayashi S, Wang Z, Bryan J, Kobayashi C, Faccio R, Sandell LJ. The type II collagen N-propeptide, PIIBNP, inhibits cell survival and bone resorption of osteoclasts via integrin-mediated signaling. Bone. 2011; 49(4):644–652. [PubMed: 21708300]
40. Lu X, Ito Y, Atsawasuwan P, Dangaria S, Yan X, Wu T, Evans CA, Luan X. Ameloblastin modulates osteoclastogenesis through the integrin/ERK pathway. Bone. 2013; 54(1):157–168. [PubMed: 23385480]
41. Chang EJ, Kim HJ, Ha J, Kim HJ, Ryu J, Park KH, Kim UH, Lee ZH, Kim HM, Fisher DE, Kim HH. Hyaluronan inhibits osteoclast differentiation via Toll-like receptor 4. J Cell Sci. 2007; 120(Pt 1):166–176. [PubMed: 17164294]
42. Lee NK, Choi YG, Baik JY, Han SY, Jeong DW, Bae YS, Kim N, Lee SY. A crucial role for reactive oxygen species in RANKL-induced osteoclast differentiation. Blood. 2005; 106(3):852–859. [PubMed: 15817678]
43. Hyeon S, Lee H, Yang Y, Jeong W. Nrf2 deficiency induces oxidative stress and promotes RANKL-induced osteoclast differentiation. Free Radic Biol Med. 2013; 65:789–799. [PubMed: 23954472]

44. Lean JM, Jagger CJ, Kirstein B, Fuller K, Chambers TJ. Hydrogen peroxide is essential for estrogen-deficiency bone loss and osteoclast formation. Endocrinology. 2005; 146(2):728–735. [PubMed: 15528306]
45. Moon HJ, Ko WK, Han SW, Kim DS, Hwang YS, Park HK, Kwon IK. Antioxidants, like coenzyme Q10, selenite, and curcumin, inhibited osteoclast differentiation by suppressing reactive oxygen species generation. Biochem Biophys Res Commun. 2012; 418(2):247–253. [PubMed: 22252298]
46. Chen XD, Dusevich V, Feng JQ, Manolagas SC, Jilka RL. Extracellular matrix made by bone marrow cells facilitates expansion of marrow-derived mesenchymal progenitor cells and prevents their differentiation into osteoblasts. J Bone Miner Res. 2007; 22(12):1943–1956. [PubMed: 17680726]
47. Atkins GJ, Bouralexis S, Haynes DR, Graves SE, Geary SM, Evdokiou A, Zannettino AC, Hay S, Findlay DM. Osteoprotegerin inhibits osteoclast formation and bone resorbing activity in giant cell tumors of bone. Bone. 2001; 28(4):370–377. [PubMed: 11336917]
48. Salbach-Hirsch J, Ziegler N, Thiele S, Moeller S, Schnabelrauch M, Hintze V, Scharnweber D, Rauner M, Hofbauer LC. Sulfated glycosaminoglycans support osteoblast functions and concurrently suppress osteoclasts. J Cell Biochem. 2014; 115(6):1101–1111. [PubMed: 24356935]
49. Sells Galvin RJ, Gatlin CL, Horn JW, Fuson TR. TGF-beta enhances osteoclast differentiation in hematopoietic cell cultures stimulated with RANKL and M-CSF. Biochem Biophys Res Commun. 1999; 265(1):233–239. [PubMed: 10548519]
50. Houde N, Chamoux E, Bisson M, Roux S. Transforming growth factor-beta1 (TGF-beta1) induces human osteoclast apoptosis by up-regulating Bim. J Biol Chem. 2009; 284(35):23397–23404. [PubMed: 19574221]
51. Yang Y, Lin H, Shen H, Wang B, Lei G, Tuan RS. Mesenchymal stem cell-derived extracellular matrix enhances chondrogenic phenotype of and cartilage formation by encapsulated chondrocytes in vitro and in vivo. Acta Biomater. 2018; doi: 10.1016/j.actbio.2017.12.043
52. Hurd SA, Bhatti NM, Walker AM, Kasukonis BM, Wolchok JC. Development of a biological scaffold engineered using the extracellular matrix secreted by skeletal muscle cells. Biomaterials. 2015; 49:9–17. [PubMed: 25725550]
53. Kim B, Ventura R, Lee BT. Functionalization of porous BCP scaffold by generating cell-derived extracellular matrix from rat bone marrow stem cells culture for bone tissue engineering. J Tissue Eng Regen Med. 2017; doi: 10.1002/term.2529

Highlights

- Stem cell-derived ECM completely inhibits osteoclastogenesis of BMMs
- Stem cell-derived ECM blocks the RANKL-induced NF-κB signaling pathway
- Decellularized ECM inhibits osteoclastogenesis via attenuation of intracellular ROS
- Fibronectin contributes to ECM-mediated anti-osteoclastogenesis
- The anti-osteoclastogenic property of ECM promotes bone regeneration

Statement of Significance

Decellularized extracellular matrix (ECM) derived from stem cells has been shown as a promising biomaterial for bone regeneration; however, bone remodeling is influenced by bone resorption and little is known about the effect of cell-derived ECM on osteoclast differentiation. Cell-derived ECM improved BMM proliferation but potently inhibited osteoclast differentiation. ECM-mediated attenuation of intracellular reactive oxygen species was suggested to play a rival role in osteoclastogenesis. Fibronectin in cell-derived ECM also contributed to ECM-mediated anti-osteoclastogenesis. The anti-osteoclastogenic property of cell-derived ECM may benefit clinically for modulating bone remodeling and promoting bone tissue engineering.

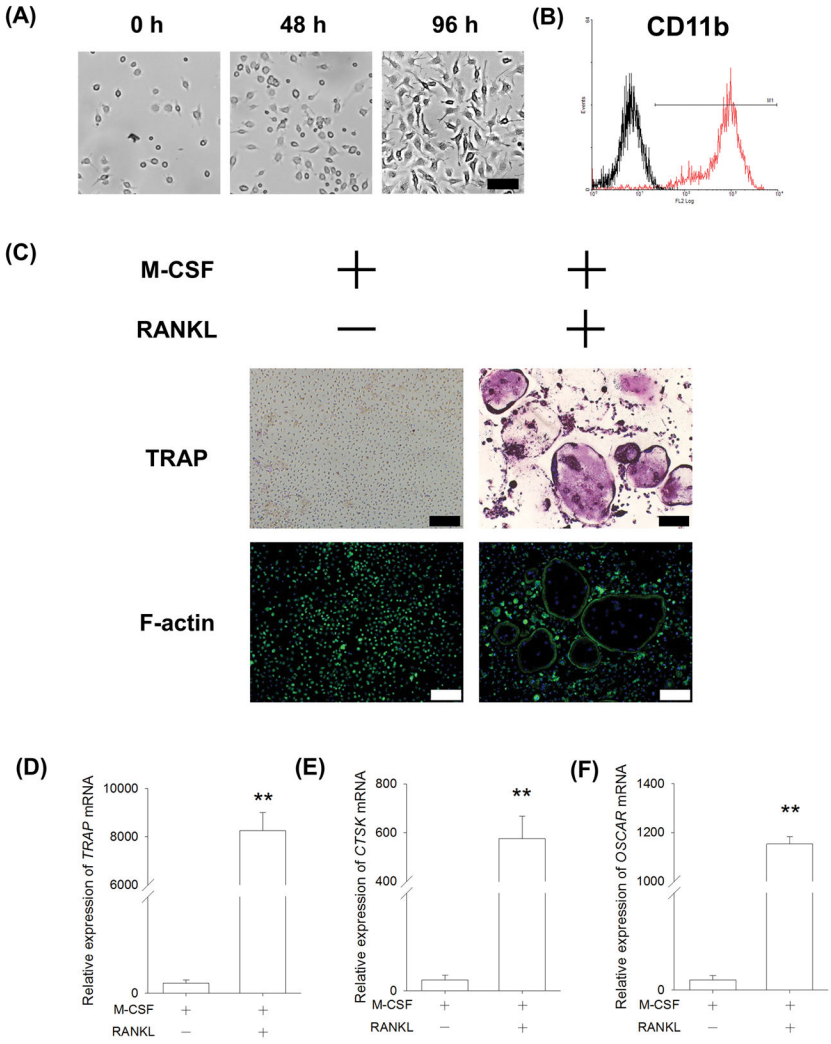

Fig. 1.

Characterization of primary BMMs isolated from C57BL/6 mice. (A) BMMs were treated with 50 ng/mL M-CSF and the cell morphology was observed in representative bright field images. Scale bar = 50 μm. (B) Primary BMMs were strongly positive for CD11b (red). IgG Isotype (black) served as a negative control. (C) *In vitro* osteoclastogenesis of BMMs was induced by 20 ng/mL M-CSF and 50 ng/mL RANKL. After a five-day induction, multinucleated osteoclasts were positively stained for TRAP and the formation of the F-actin ring was assessed using immunofluorescence staining with phalloidin. Cell nuclei were counterstained with DAPI. Scale bar = 200 μm. (D–F) The mRNA levels of *TRAP* (D), *CTSK* (E), and *OSCAR* (F) were measured by real-time RT-PCR. Values are the mean ± S.E.M. of four independent experiments ($n = 4$). Statistically significant differences are indicated by * $p < 0.05$ or ** $p < 0.01$ between the indicated groups.

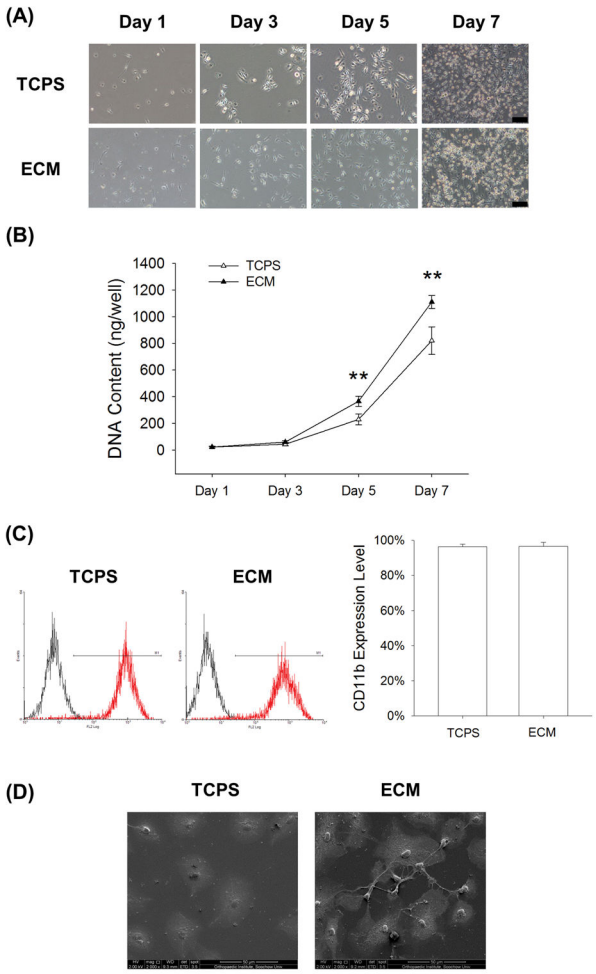

Fig. 2.

The effect of cell-derived ECM on cell proliferation of BMMs. Cells were cultured on the standard TCPS or ECM-coated substrate and treated with 20 ng/mL M-CSF. (A) The cell density of BMMs cultured on TCPS or ECM was observed after a 96-h culture. Scale bar = 100 μm. (B) At separate time points of Days 1, 3, 5, and 7, cell proliferation was quantified and decellularized ECM improved the cell growth of BMMs compared to the TCPS group. (C) The expression levels of CD11b in TCPS-cultured and ECM-cultured BMMs were analyzed by flow cytometry. (D) The cell morphology of BMMs cultured on TCPS or ECM was observed by SEM. Scale bar = 50 μm. Values are presented as the mean ± S.E.M. and each experiment was carried out with four replicates ($n = 4$). Statistically significant differences are indicated by * $p < 0.05$ or ** $p < 0.01$ between the indicated groups.

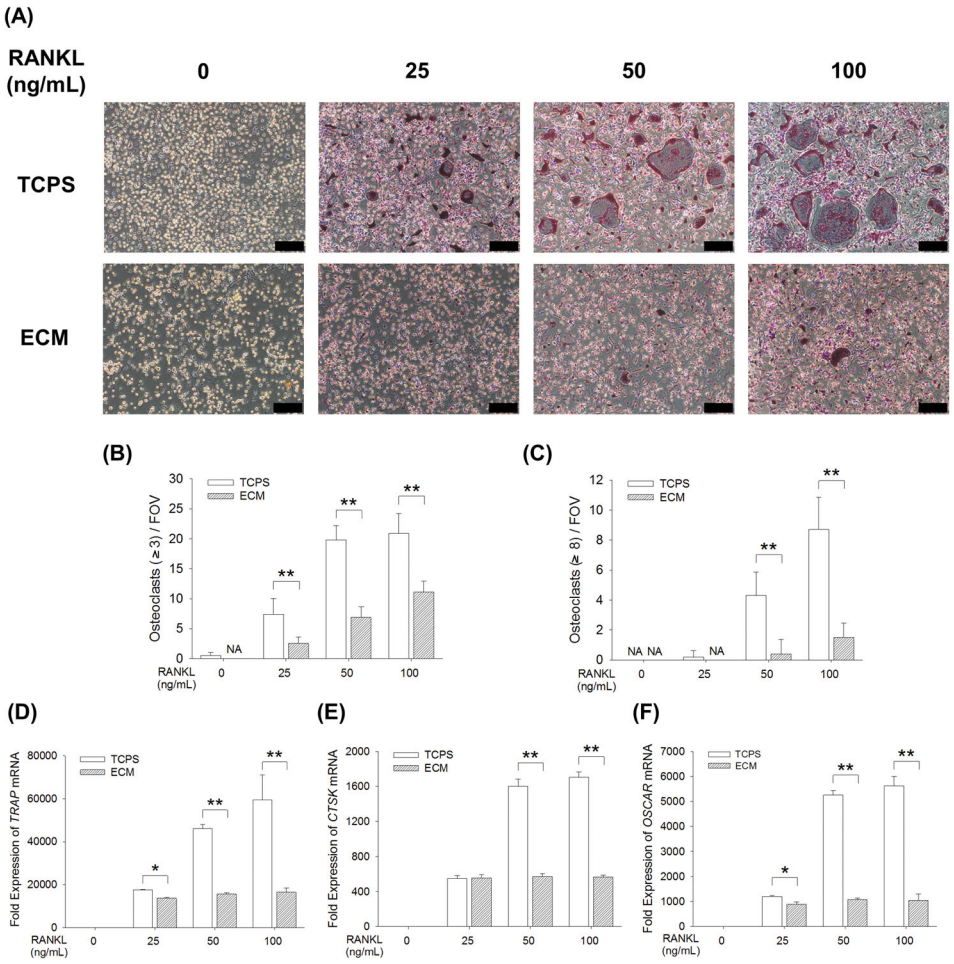

Fig. 3.

Cell-derived ECM inhibited *in vitro* osteoclastogenesis of BMMs. BMMs were cultured on the standard TCPS or ECM-coated substrate and induced toward osteoclasts by 25 ng/mL, 50 ng/mL, or 100 ng/mL RANKL, supplemented with 20 ng/mL M-CSF. (A) After a five-day culture, multinucleated osteoclasts were positively stained for TRAP and the nuclei were counterstained with DAPI (three replicates for each treatment). Scale bar = 200 μm. (B–C) Quantification of the cell number of TRAP-positive osteoclasts with greater than 3 nuclei (B) and with 8 or more nuclei (C). TRAP-positive osteoclasts were counted in at least ten randomly chosen fields of view (FOV). (D–F) The mRNA levels of *TRAP* (D), *CTSK* (E), and *OSCAR* (F) were measured by real-time RT-PCR. Values are presented as the mean ± S.E.M. of four independent experiments ($n = 4$). Statistically significant differences are indicated by * $p < 0.05$ or ** $p < 0.01$ between the indicated groups.

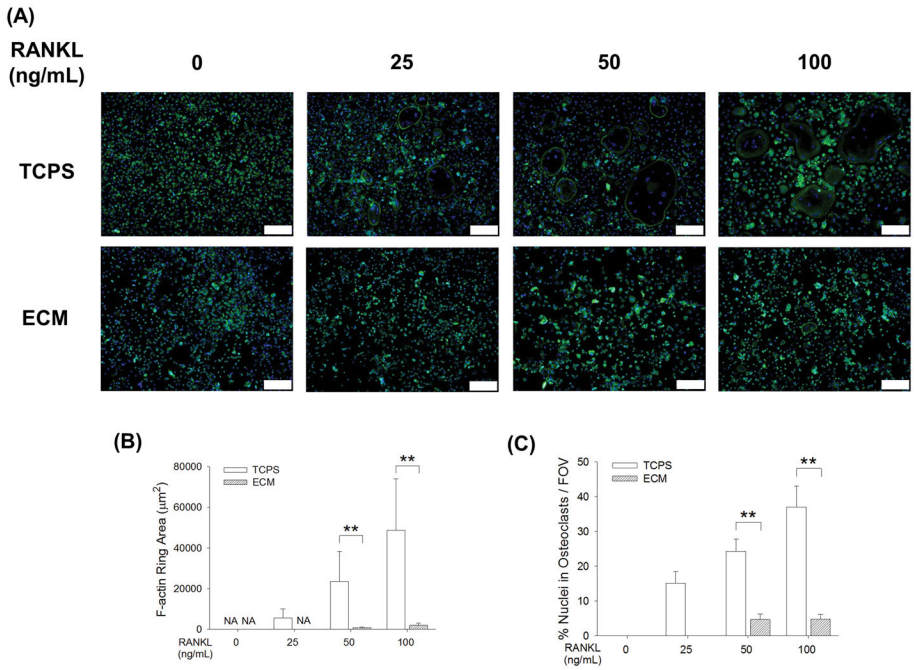

Fig. 4.

Decellularized ECM suppressed the formation of the F-actin ring in osteoclasts. (A) After a five-day induction, the F-actin rings were labeled with phalloidin and the nuclei were counterstained with DAPI. Scale bar = 200 μm. (B) The area of F-actin rings of the ECM-cultured osteoclasts was significantly smaller than the TCPS-cultured cells. (C) The percent nuclei in F-actin was expressed as an index for fusion efficiency, which was calculated as nuclei within F-actin rings divided by total nuclei. A significantly decreased fusion efficiency was observed in the ECM-cultured BMMs. Multinucleated osteoclasts were counted in at least ten randomly chosen fields of view (FOV). Values are presented as the mean ± S.E.M. of four independent experiments ($n = 4$). Statistically significant differences are indicated by * $p < 0.05$ or ** $p < 0.01$ between the indicated groups.

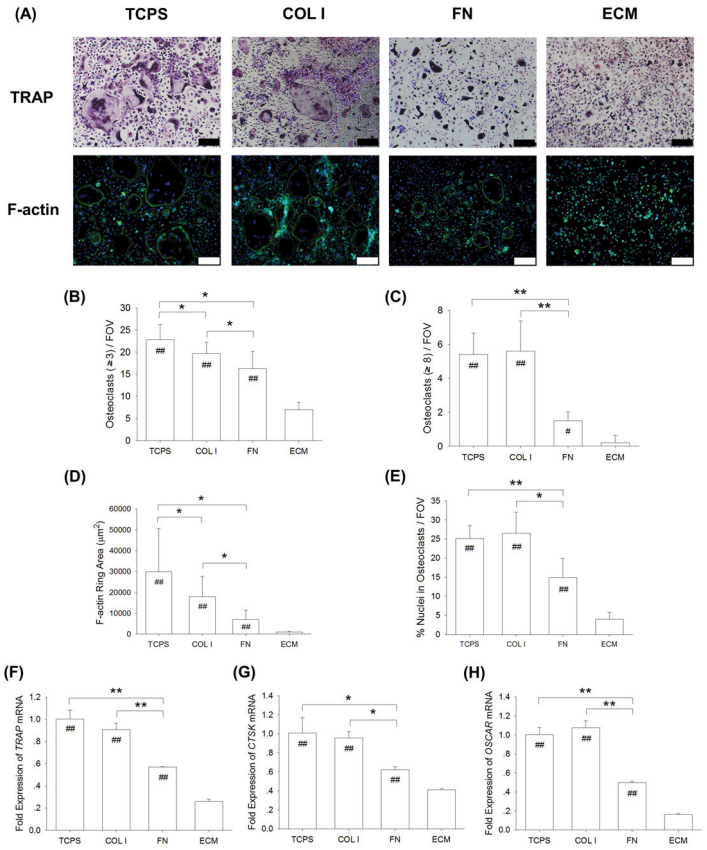

Fig. 5.

The role of matrix proteins in modulating osteoclastogenesis. BMMs were induced toward osteoclasts on TCPS, COL I, FN, and DECM by treating with 20 ng/mL M-CSF and 50 ng/mL RANKL. (A) After a five-day culture, multinucleated osteoclasts were positively stained for TRAP and the F-actin rings were labeled with phalloidin. Cell nuclei were counterstained with DAPI (three replicates for each treatment). Scale bar = 200 μm. (B–C) Quantification of the cell number of TRAP-positive osteoclasts with greater than 3 nuclei (B) and with 8 or more nuclei (C). TRAP-positive osteoclasts were counted in at least ten randomly chosen fields of view (FOV). (D–E) The area of F-actin rings (D) and the percent nuclei in F-actin as an index for fusion efficiency (E) were quantified. Multinucleated osteoclasts were counted in at least ten randomly chosen fields of view (FOV). (F–H) The mRNA levels of *TRAP* (F), *CTSK* (G), and *OSCAR* (H) were measured by real-time RT-PCR. Values are presented as the mean ± S.E.M. of four independent experiments ($n = 4$). Statistically significant differences are indicated by * $p < 0.05$ or ** $p < 0.01$ between the indicated groups. Statistically significant differences are indicated by $^{\#}$ $p < 0.05$ or $^{\#\#}$ $p < 0.05$ vs. the ECM group.

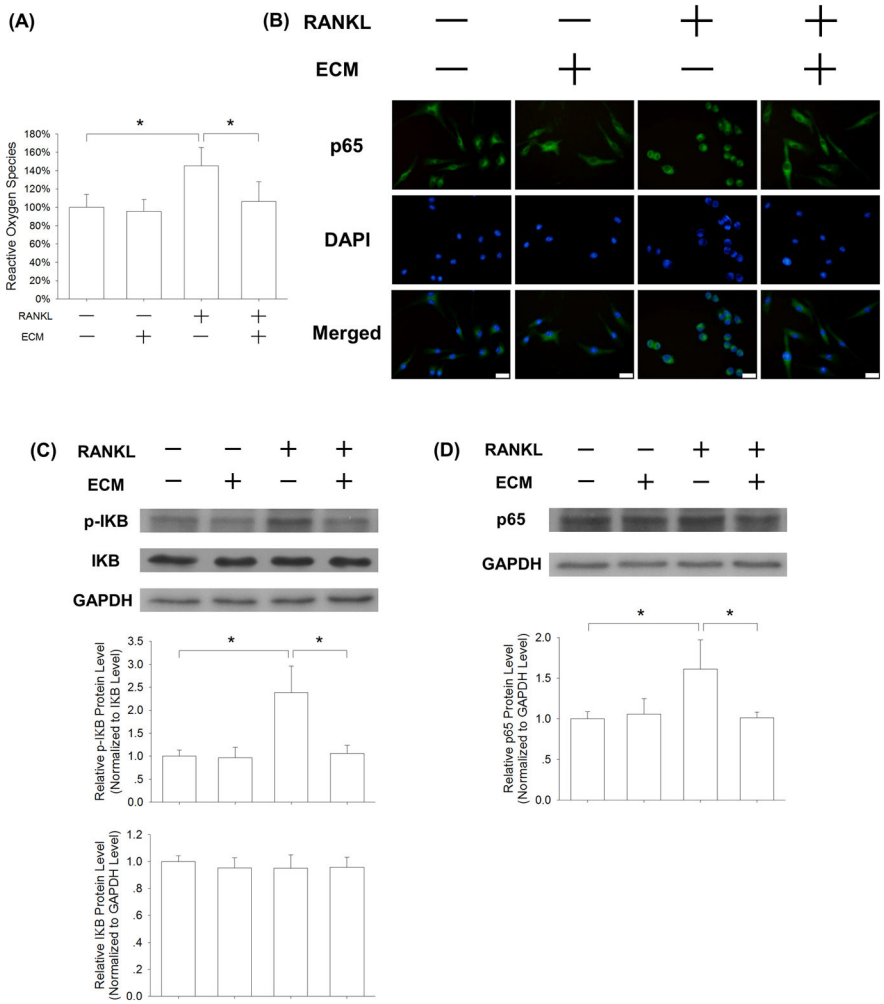

Fig. 6.

Cell-derived ECM inhibited osteoclastogenesis of BMMs via attenuation of RANKL-induced ROS production. BMMs were cultured on the standard TCPS or ECM-coated substrate and treated with 20 ng/mL M-CSF and 50 ng/mL RANKL. (A) After a 24-h culture, the levels of intracellular ROS in the TCPS-cultured and ECM-cultured BMMs were measured. (B) Representative immunofluorescence staining images of the NF-κB signaling pathway. RANKL treatment induced nuclear localization of p65 in the TCPS-cultured BMMs, but failed to induce translocation in the ECM-cultured cells, indicating that ECM inhibited the activation of the NF-κB signaling pathway. Scale bar = 20 μm. (C) Western blot assay showed that cell-derived ECM inhibited NF-κB activation by suppressing phosphorylation of IκB. (D) The protein levels of p65 were evaluated in the TCPS-cultured and ECM-cultured BMMs. The GAPDH lane served as a loading control. Values are the mean ± S.E.M. of three independent experiments ($n = 3$). Statistically significant differences are indicated by * $p < 0.05$ or ** $p < 0.01$ between the indicated groups.

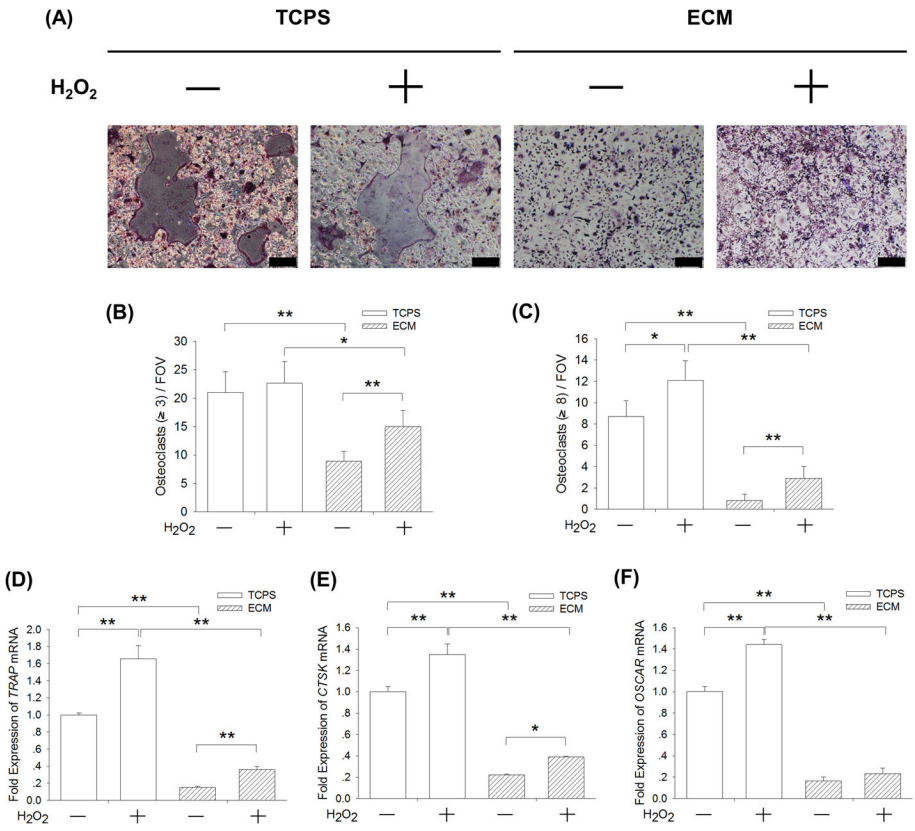

Fig. 7.

Supplementation with exogenous H_2O_2 partially rescued ECM-inhibited osteoclastogenesis. BMMs were cultured on cell-derived ECM and induced toward osteoclasts with or without the addition of 20 μM H_2O_2. (A) Multinucleated osteoclasts were positively stained for TRAP and cell nuclei were counterstained with DAPI (three replicates for each treatment). Scale bar = 200 μm. (B–C) Quantification of the cell number of TRAP-positive osteoclasts with greater than 3 nuclei (B) and with 8 or more nuclei (C). TRAP-positive osteoclasts were counted in at least ten randomly chosen fields of view (FOV). (D–F) The mRNA levels of *TRAP* (D), *CTSK* (E), and *OSCAR* (F) were measured by real-time RT-PCR. Values are presented as the mean ± S.E.M. of four independent experiments ($n = 4$). Statistically significant differences are indicated by * $p < 0.05$ or ** $p < 0.01$ between the indicated groups.

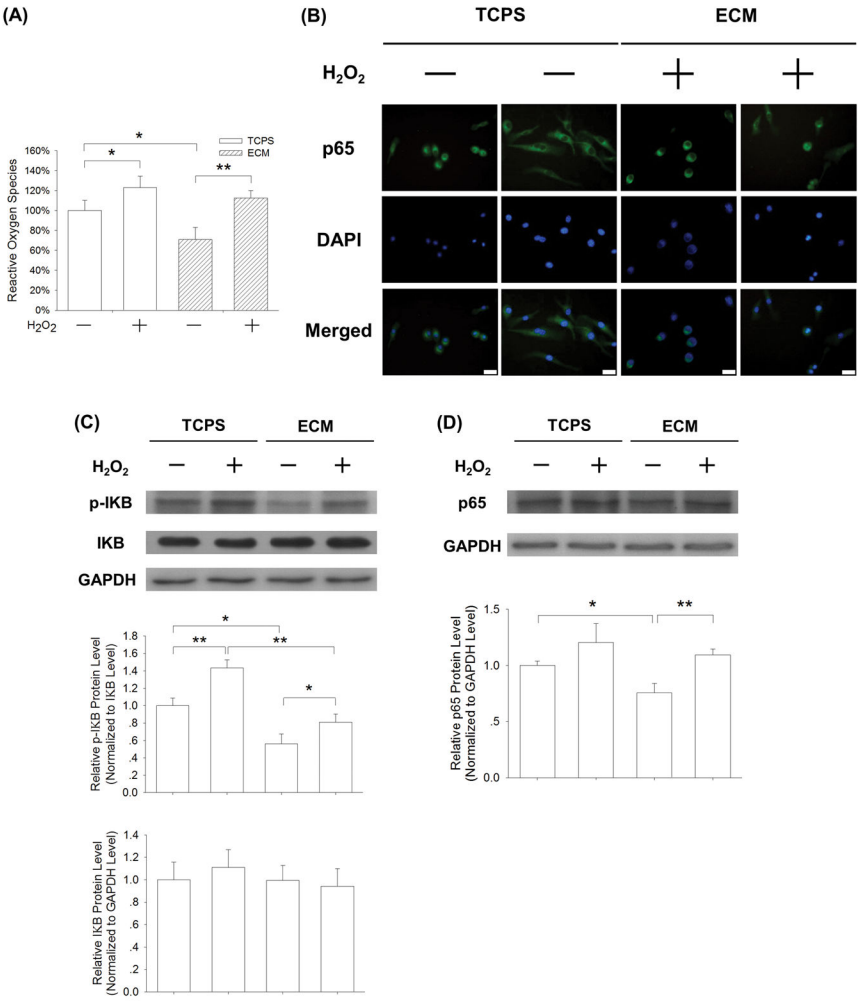

Fig. 8.

Supplementation with exogenous H_2O_2 activated the ECM-inhibited NF-κB signaling pathway. BMMs were cultured on cell-derived ECM and induced toward osteoclasts with or without the addition of 20 μM H_2O_2. (A) After a 24-h exposure to exogenous H_2O_2, the flow cytometry assay showed an increase in intracellular ROS in the ECM-cultured BMMs. Values are presented as the mean ± S.E.M. and each experiment was carried out with four replicates ($n = 4$). (B) Addition of exogenous H_2O_2 resulted in the translocation of p65 from the cytoplasm into the nucleus in the ECM-cultured BMMs. Scale bar = 20 μm. (C) The phosphorylation of IκB was enhanced by treatment with exogenous H_2O_2. (D) The protein levels of p65 were up-regulated by treatment with exogenous H_2O_2. The GAPDH lane served as a loading control. Values are the mean ± S.E.M. of three independent experiments ($n = 3$). Statistically significant differences are indicated by * $p < 0.05$ or ** $p < 0.01$ between the indicated groups.

Table 1

Primers used for Real-time RT-PCR

Gene	Forward Primer sequence(5′-3′)	Reverse Primer sequence(5′-3′)
GAPDH	AGGTCGGTGTGAACGGATTTG	TGTAGACCATGTAGTTGAGGTCA
TRAP	ACTTGCGACCATTGTTAGCC	AGAGGGATCCATGAAGTTGC
CTSK	AGCAGAACGGAGGCATTGACTC	TTTAGCTGCCTTTGCCGTGGC
OSCAR	TGGCGGTTTGCACTCTTCA	GATCCGTTACCAGCAGTTCCAGA